

## Fourier two-level analysis for discontinuous Galerkin discretization with linear elements

P. W. Hemker<sup>1,\*</sup>,<sup>†</sup>, W. Hoffmann<sup>2</sup> and M. H. van Raalte<sup>2</sup>

<sup>1</sup>*CWI, Amsterdam, The Netherlands*

<sup>2</sup>*KdV Institute for Mathematics, University of Amsterdam, The Netherlands*

### SUMMARY

In this paper we study the convergence of a multigrid method for the solution of a linear second-order elliptic equation, discretized by discontinuous Galerkin (DG) methods, and we give a detailed analysis of the convergence for different block-relaxation strategies. To complement an earlier paper where higher-order methods were studied, here we restrict ourselves to methods using piecewise linear approximations. It is well known that these methods are unstable if no additional interior penalty is applied.

As for the higher-order methods, we find that point-wise block-relaxations give much better results than the classical cell-wise relaxations. Both for the Baumann–Oden and for the symmetric DG method, with a sufficient interior penalty, the block-relaxation methods studied (Jacobi, Gauss–Seidel and symmetric Gauss–Seidel) all make excellent smoothing procedures in a classical multigrid setting. Independent of the mesh size, simple MG cycles give convergence factors 0.2–0.4 per iteration sweep for the different discretizations studied. Copyright © 2004 John Wiley & Sons, Ltd.

KEY WORDS: discontinuous Galerkin method; multigrid iteration; two-level Fourier analysis; point-wise block-relaxation

### 1. INTRODUCTION

Recently renewed interest arose in discontinuous Galerkin (DG) discretizations for partial differential equations of convection diffusion type [1–3]. An important reason is the new insight in the use of these methods for elliptic equations [4–6] and their applicability in *hp*-self-adaptive algorithms [7, 8].

However, thus far relatively little attention has been paid to optimally efficient solution methods for the algebraic systems arising from the discretization of the stationary problems. Therefore, we study the possible use of a multigrid algorithm for this purpose. We concentrate on the Baumann DG, the symmetric DG methods [4, 9]. It is well known [10–12] that these methods are not stable for the lowest order of approximation ( $p = 1$ ), if no additional stabilization is applied by means of an interior penalty (IP) parameter. All these methods can

\*Correspondence to: P. W. Hemker, CWI, P.O. Box 94079, 1090 GB Amsterdam, The Netherlands.

<sup>†</sup>E-mail: p.w.hemker@cwi.nl

be described by the same formulas [4, 9], where the distinction between the various methods is made by two parameters:  $\sigma$ , the sign ( $\sigma = +1$  for Baumann and  $\sigma = -1$  for symmetric DG), and  $\mu = \nu/h$ , the IP parameter.

Whereas in an earlier paper [9] we studied the convergence of a multigrid method for the solution of the systems arising from higher-order methods ( $p \geq 3$ ), in the present paper we focus on the convergence of the multigrid method for the case  $p = 1$ , because this case may be used to accelerate the solution for  $p > 1$  in the  $p$ -hierarchical structure of the  $hp$ -adaptive approximation process.

For the higher-order methods we showed that excellent convergence was obtained when block-wise relaxation (Jacobi or Gauss–Seidel) is applied as a smoother, if the blocks are formed by the degrees of freedom (d.o.f.’s) associated with cell-vertices [9]. This motivates us to study the smoothing abilities for the IP-DG method with a well-chosen penalty parameter  $\mu$ .

The outline of the paper is as follows. In Section 2 we give a unified description of the DG discretizations so that the symmetric form, Baumann’s variant and the IP variants follow from the values of specific parameters ( $\sigma$  and  $\mu$ ) in the formulation. For the linear trial functions that we restrict ourselves to, we give a description of the resulting discrete operator in the form of a stencil that defines the resulting block-Toeplitz matrix.

In Section 3 we apply Fourier analysis to this discrete operator in order to study its stability properties. We observe that both the symmetric DG and Baumann’s variant have a double zero eigenvalue, one of which has an eigenfunction that is not constant (the spurious eigenvalue responsible for the instability of the methods). If a large enough penalty parameter is chosen, then it is seen that the instability disappears. However, for too large a value of the penalty parameter we see that the discrete system becomes ill-conditioned.

In Section 4 we give a smoothing analysis of the point-wise and cell-wise block-relaxations and a convergence analysis of the two-level algorithm. As in the case of higher degree trial polynomials, dealt with in our earlier paper, we see also here that the use of point-wise relaxation gives much faster convergence. By determining the spectral norm of the error-amplification operator it is shown that the observed ‘good convergence’ is guaranteed from the second iteration step on. We find convergence with a rate of about 0.2–0.4/iteration.

In Section 5 we report on numerical results for the solution of a one-dimensional Poisson problem on the unit interval, where the solution has a thin boundary layer, its thickness depending on a parameter  $\varepsilon$ . The results confirm the theoretical analysis.

## 2. THE LINEAR DISCONTINUOUS GALERKIN DISCRETIZATION

We consider the Poisson equation on the unit cube  $\Omega$ , partly with Neumann and partly with Dirichlet boundary conditions

$$-\Delta u = f \quad \text{on } \Omega$$

with  $u = u_0$  on  $\Gamma_D$  and  $\mathbf{n} \cdot \nabla u = g$  on  $\Gamma_N$ , where  $\Gamma_D \cap \Gamma_N = \emptyset$  and  $\bar{\Gamma}_D \cup \bar{\Gamma}_N = \partial\Omega$  and  $\Gamma_D \neq \emptyset$ . The variational form of this equation, associated with the DG-methods [4, 9] reads: find  $u \in H^1(\Omega_h)$  such that

$$B(u, v) = L(v) \quad \forall v \in H^1(\Omega_h) \tag{1}$$

where

$$\begin{aligned}
 B(u, v) = & \sum_{\Omega_e \in \Omega_h} \int_{\Omega_e} \nabla u \cdot \nabla v \, dx - \int_{\Gamma_{\text{int}} \cup \Gamma_{\text{D}}} \langle \nabla u \rangle \cdot [v] \, ds \\
 & + \sigma \int_{\Gamma_{\text{int}} \cup \Gamma_{\text{D}}} \langle \nabla v \rangle \cdot [u] \, ds + \mu \int_{\Gamma_{\text{int}}} [u] \cdot [v] \, ds
 \end{aligned} \tag{2}$$

and

$$L(v) = \sum_{\Omega_e \in \Omega_h} \int_{\Omega_e} f v \, dx + \sigma \int_{\Gamma_{\text{D}}} \langle \nabla v \rangle \cdot [u_0] \, ds + \int_{\Gamma_{\text{N}}} g v \, ds$$

Here, for non-negative integer  $k$ , the space  $H^k(\Omega_h)$  is the broken Sobolev space [5] on the partitioning  $\Omega_h$  of the domain  $\Omega$ ,

$$\Omega_h = \{ \Omega_e | \cup_e \bar{\Omega}_e = \bar{\Omega}, \Omega_i \cap \Omega_j = \emptyset, i \neq j \}$$

The parameter  $\mu$  denotes the IP, and  $\sigma$  the character of the discretization:  $\sigma = 1$  gives Baumann’s method (or NIPG if  $\mu > 0$ ),  $\sigma = -1$  gives the symmetric DG (IP-DG for  $\mu > 0$ ). The jump operator  $[\cdot]$  and the average operator  $\langle \cdot \rangle$  are defined at the common interface between two cells  $\Gamma_{i,j} = \bar{\Omega}_i \cap \bar{\Omega}_j$ , by

$$\begin{aligned}
 [w(x)] = & w(x)|_{\partial\Omega_i, \mathbf{n}_i} + w(x)|_{\partial\Omega_j, \mathbf{n}_j} \\
 \langle w(x) \rangle = & \frac{1}{2}(w(x)|_{\partial\Omega_i} + w(x)|_{\partial\Omega_j})
 \end{aligned} \tag{3}$$

for  $x \in \Gamma_{i,j}$ . Here  $\mathbf{n}_i$  is the unit outward pointing normal for cell  $\Omega_i$ . For the jump operator at a Dirichlet boundary the interface with a virtual (flat, exterior) adjacent cell, containing only the Dirichlet data, is used. In case of a vector-valued function,  $\tau$ , we define

$$\begin{aligned}
 [\tau(x)] = & \tau(x)|_{\partial\Omega_i} \cdot \mathbf{n}_i + \tau(x)|_{\partial\Omega_j} \cdot \mathbf{n}_j \\
 \langle \tau(x) \rangle = & \frac{1}{2}(\tau(x)|_{\partial\Omega_i} + \tau(x)|_{\partial\Omega_j})
 \end{aligned} \tag{4}$$

The interior boundaries are denoted by  $\Gamma_{\text{int}} = \bigcup \Gamma_{i,j}$ .

In this paper we study the one-dimensional equation, since this can be considered as an essential building block for the higher dimensional case where we use tensor product polynomials. For test and trial space  $S_h \subset H^1(\Omega_h)$  we use the space of discontinuous piecewise polynomials on the partitioning  $\Omega_h$ . Then the discrete equations read: find  $u_h \in S_h$  such that

$$B(u_h, v_h) = L(v_h) \quad \forall v_h \in S_h \tag{5}$$

With a basis  $\{\phi_{i,e}\}$  for the space  $S_h$  this leads to the linear system

$$\begin{aligned}
 & \sum_{e=1}^N \sum_{i=0}^1 c_{i,e} \left( \int_{\Omega_e} \phi'_{i,e}(x) \phi'_{j,e}(x) \, dx - \langle \phi'_{i,e}(x) \rangle \cdot [\phi_{j,e}(x)]|_{\Gamma_{\text{int}} \cup \Gamma_{\text{D}}} \right. \\
 & \quad \left. + \sigma [\phi_{i,e}(x)] \cdot \langle \phi'_{j,e}(x) \rangle|_{\Gamma_{\text{int}} \cup \Gamma_{\text{D}}} + \mu [\phi_{i,e}(x)] \cdot [\phi_{j,e}(x)]|_{\Gamma_{\text{int}}} \right) \\
 & = \sum_{e=1}^N \sum_{i=0}^1 \int_{\Omega_e} f \phi_{j,e}(x) \, dx + \sigma [u_0] \cdot \langle \phi'_{j,e}(x) \rangle|_{\Gamma_{\text{D}}} + g \phi_{j,e}(x)|_{\Gamma_{\text{N}}}
 \end{aligned} \tag{6}$$

which we briefly denote by  $L_h u_h = f_h$ . In this paper we restrict ourselves to  $S_h$  consisting of piecewise linear polynomials on a uniform partitioning for which we use the element basis functions  $\phi_j(\xi) = \xi^j(1 - \xi)^{1-j}$ ,  $j = 0, 1$ , so that we have  $2N$  basis functions  $\phi_j((x - x_e)/h) = \phi_{j,e}(x)$ ;  $j = 0, 1$ ;  $e = 1, \dots, N$ . For this basis of piecewise linear polynomials the linear system (6) has a  $2 \times 2$ -block-tridiagonal structure, with the discretization stencil

$$\frac{1}{h} \left[ \begin{array}{cc|cc|cc} -\frac{1}{2} & \frac{1-\sigma}{2} - h\mu & \frac{1+\sigma}{2} + h\mu & \frac{-1-\sigma}{2} & \frac{1}{2}\sigma & 0 \\ 0 & \frac{1}{2}\sigma & \frac{-1-\sigma}{2} & \frac{1+\sigma}{2} + h\mu & \frac{1-\sigma}{2} - h\mu & -\frac{1}{2} \end{array} \right] \tag{7}$$

if the equations (the weighting functions  $\phi_{e,j}$ ) and coefficients are ordered *cellwise* as  $[c_{e,0}, c_{e,1}]_{e=1}^N$ . As we emphasized in Reference [9] we can also order the equations and coefficients *pointwise*, according to function values at the cell-interfaces,  $[c_{e-1,1}, c_{e,0}]_{e=2}^N$ , which leads to the stencil

$$\frac{1}{h} \left[ \begin{array}{cc|cc|cc} \frac{1}{2}\sigma & \frac{-1-\sigma}{2} & \frac{1+\sigma}{2} + h\mu & \frac{1-\sigma}{2} - h\mu & -\frac{1}{2} & 0 \\ 0 & -\frac{1}{2} & \frac{1-\sigma}{2} - h\mu & \frac{1+\sigma}{2} + h\mu & \frac{-1-\sigma}{2} & \frac{1}{2}\sigma \end{array} \right] \tag{8}$$

Thus, with the possible exception for the equations at the boundaries, the discretization matrix appears to be a block-Toeplitz matrix and is described by the repetition of either stencil (7) or stencil (8). Both stencils describe one and the same matrix, but the distinction between cell-wise and point-wise blocks materializes as soon as we consider block-relaxation methods.

### 3. FOURIER ANALYSIS OF THE DISCRETE OPERATOR $B(u_h, v_h)$

In this section we first introduce the Fourier transform of a block-Toeplitz operator. We describe the spectrum of the discrete operator  $L_h$  on an infinite domain, and we discuss its stability properties. We notice the difference between this operator for piecewise cubic approximations, as described in Reference [9], and the corresponding operator for piecewise linears. We recognize that for the latter a sufficiently large IP parameter has to be chosen in order to obtain a stable scheme. Then, for the stable schemes, we compute the order of accuracy.

#### 3.1. Fourier analysis for a block-Toeplitz operator $A_h$

In Reference [9] we have shown that, for  $A_h = (\mathbf{a}_{m,j}) \in \mathbb{R}^{2\mathbb{Z} \times 2\mathbb{Z}}$  an infinite block-Toeplitz operator, we have the identity

$$\sum_{j \in \mathbb{Z}} \mathbf{a}_{m,j} e_{h,\omega}(jh) = \hat{A}_h(\omega) e_{h,\omega}(mh)$$

with

$$\hat{A}_h(\omega) = \sum_{j \in \mathbb{Z}} \mathbf{a}_{m,j} e^{i(j-m)h\omega} = \sum_{k \in \mathbb{Z}} \mathbf{a}_{-k} e^{ikh\omega} = \sum_{k \in \mathbb{Z}} \mathbf{a}_k e^{-ikh\omega} \tag{9}$$

Table I. Eigenvalues of  $\widehat{L}_h(\omega)$ .

$\lambda_h(\omega)$	Baum-DG $\sigma = 1, \mu = 0$	Symm-DG $\sigma = -1, \mu = 0$	IP-DG $\sigma = -1, \mu = v/h$
$\lambda_1(\omega)$	$\frac{1 + \cos(\omega h)}{h}$	$\frac{1 - \cos(\omega h)}{h}$	$\frac{v - \cos(\omega h) +  v - 1 }{h}$
$\lambda_2(\omega)$	$\frac{1 - \cos(\omega h)}{h}$	$\frac{-1 - \cos(\omega h)}{h}$	$\frac{v - \cos(\omega h) -  v - 1 }{h}$

for all  $\omega \in \mathbb{T}_h \equiv [-\pi/h, \pi/h]$ . Here  $e_{h,\omega}(jh) = e^{ijh\omega}$  is an elementary mode, defined on the regular infinite one-dimensional grid

$$\mathbb{Z}_h = \{jh \mid j \in \mathbb{Z}, h > 0\}$$

Furthermore, with  $V_h = V_h(\omega)$  the matrix of eigenvectors  $\mathbf{v}(\omega)$  of  $\widehat{A}_h(\omega)$ , such that

$$\widehat{A}_h(\omega)V_h = V_h\Lambda_h(\omega) \tag{10}$$

then, with  $(V_h \otimes e_{h,\omega})(jh) = V_h(\omega)e^{ijh\omega}$ , we have

$$A_h(V_h \otimes e_{h,\omega}) = \widehat{A}_h(\omega)(V_h \otimes e_{h,\omega}) = (V_h \otimes e_{h,\omega})\Lambda_h(\omega) \tag{11}$$

Hence, the columns  $\mathbf{v}(\omega)e_{h,\omega}(mh)$  of  $V_h \otimes e_{h,\omega}$  are the eigenvectors of  $A_h$  and  $\Lambda_h(\omega)$  is a family of  $2 \times 2$  diagonal matrices containing the eigenvalues of  $A_h$  on its diagonal.

### 3.2. Eigenvalues spectra of the discrete operator $L_h$

Now we study the eigenvalue spectra of the discrete operator  $L_h$  of (i) Baumann’s, (ii) the symmetric-, and (iii) the IP-DG-method, all with linear elements. It is well known that in this case Baumann’s and the symmetric DG-method are unstable and that an additional penalty parameter  $\mu = v/h$  (IP-DG-method) can be introduced in order to stabilize the discrete operator  $L_h$ . To study the behavior of the three different DG-methods we look at the eigenvalue spectra of  $\widehat{L}_h(\omega)$ , since the eigenvalues and eigenvectors of  $\widehat{L}_h(\omega)$  correspond with the eigenvalues and eigenvectors of  $L_h$ . Considering the point-wise stencil (8) we write for  $\widehat{L}_h(\omega)$ , using (9),

$$\widehat{L}_h(\omega) = \frac{1}{2h} \begin{pmatrix} 1 + \sigma + 2v - e^{\omega h} + \sigma e^{-\omega h} & 1 - \sigma - 2v - (1 + \sigma)e^{-\omega h} \\ 1 - \sigma - 2v - (1 + \sigma)e^{\omega h} & 1 + \sigma + 2v - e^{-\omega h} + \sigma e^{\omega h} \end{pmatrix} \tag{12}$$

The eigenvalues  $\lambda_h(\omega)$  of  $\widehat{L}_h(\omega)$  for, respectively, Baumann’s, the symmetric and the IP-DG-method are shown in Table I. Note that the same eigenvalues are obtained if the cell-wise stencil (7) is used instead of the point-wise stencil (8). Only the coefficients of the eigenvectors  $\mathbf{v}(\omega)e_{h,\omega}(mh)$  are collected either point-wise ( $[c_{e-1,1}, c_{e,0}]$ ) or cell-wise ( $[c_{e,0}, c_{e,1}]$ ).

If we study the eigenvalues  $\lambda_h(\omega)$  of  $\widehat{L}_h(\omega)$  for Baumann’s DG-method, we see in Table I that they are real and non-negative:  $\lambda_1(\omega), \lambda_2(\omega) \in [0, 2/h]$ . Furthermore we see that  $\lambda_2 = 0$  for  $\omega = 0$ , which is the eigenvalue corresponding to the constant eigenfunction. This eigenfunction corresponds to the equivalent eigenfunction for the continuous operator and is controlled by the boundary conditions. However, we see that there also is an additional zero eigenvalue

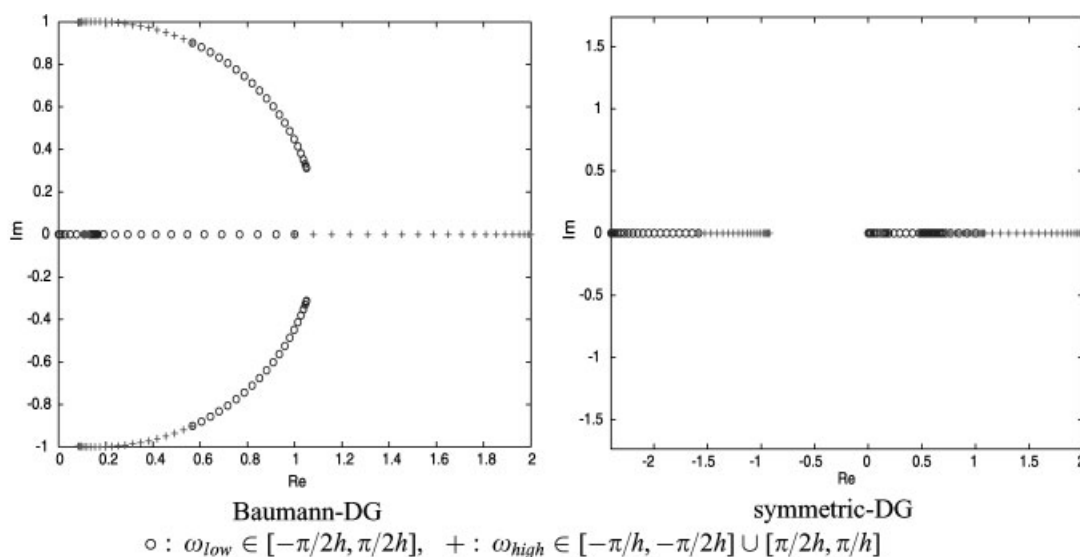


Figure 1. Eigenvalue spectra of discrete operator  $\widehat{L}_h(\omega)$  for cubic stencil.

$\lambda_1 = 0$  for  $\omega = \pm\pi/h$ , and the corresponding eigenvector is oscillating piecewise constant. This spurious zero eigenvalue causes the Baumann DG-method to be singular for linear basis functions in the test and trial space.

The same oscillating piecewise constant function is an additional eigenfunction, with  $\lambda_2 = 0$ , for the discrete operator  $L_h$  for the symmetric DG-method. Furthermore, for this DG-method we recognize the saddle-point behavior  $\lambda_1(\omega) \in [0, 2/h]$ ,  $\lambda_2(\omega) \in [-2/h, 0]$ .

If we study the eigenvalue spectrum  $\lambda_h(\omega)$  for the IP-DG-method, then we may still choose the penalty parameter  $\nu$ . If we choose  $\nu < 0$ , the method is stable in the sense that the unique zero eigenvalue corresponds to the constant eigenfunction. However, the method is indefinite. If we choose the parameter  $0 \leq \nu < 1$  the method is indefinite *and* unstable (since then there is a spurious zero eigenvalue with a corresponding oscillating piecewise constant eigenfunction). For  $\nu \geq 1$  the method is stable (the eigenvalues have non-negative sign). On the other hand, for a large parameter  $\nu$  the discrete operator is ill-conditioned.

Whereas, for linear polynomials in the test and trial space, Baumann's non-symmetric DG-method has positive real eigenvalues, this is not the case for higher-order piecewise polynomials (although they have positive real parts). Figure 1 shows the eigenvalue spectra of the Baumann and the symmetric DG-methods for piecewise cubics, as analyzed in Reference [9]. The spectrum of Baumann's method shows complex eigenvalues; in the case of the symmetric DG-method the spectrum is real but indefinite. Notice the distinction between eigenvalues for low and high frequencies which is useful in the context of multigrid. (Low frequency functions can also be represented on a twice coarser grid.)

### 3.3. Consistency of the IP-DG-method

In the previous section we have seen that the IP-DG-method for the piecewise linear basis is stable if  $\nu \geq 1$ . In this section we study the accuracy and the discrete convergence of this

method. For the analysis we use the point-wise stencil (8) and proceed analogously to the treatment in Reference [9], and we study the truncation operator

$$\tau_h = L_h R_h - \bar{R}_h L \tag{13}$$

and the operator corresponding with the discrete convergence,  $C_h = L_h^{-1} \tau_h$ . In (13)  $R_h : C^1(\Omega_h) \rightarrow \mathbb{R}^{2\mathbb{Z}_h}$  is the injective restriction defined by

$$\mathbf{u}_h(jh) = (R_h u)(jh) = \begin{bmatrix} u(jh)|_{\Omega_{j-1}} \\ u(jh)|_{\Omega_j} \end{bmatrix}$$

The second restriction,  $\bar{R}_h : C^1(\Omega_h) \rightarrow \mathbb{R}^{2\mathbb{Z}_h}$ , is the Galerkin restriction defined by

$$(\bar{R}_h f)(jh) = \begin{bmatrix} \int_{(j-1)h}^{jh} \phi_{1,j-1}(x) f(x) dx \\ \int_{jh}^{(j+1)h} \phi_{0,j}(x) f(x) dx \end{bmatrix}$$

for all  $f \in L^2(\Omega)$ . Using  $\tau_h e_\omega$  for the truncation error

$$\tau_h e_\omega(x) = \tau_h e^{i\omega x} = (L_h R_h e_\omega - \bar{R}_h L e_\omega)(x)$$

and with the definition of  $R_h$ , we find

$$\tau_h e_\omega = L_h e^{i\omega jh} \begin{bmatrix} 1 \\ 1 \end{bmatrix} - \omega^2 h e^{i\omega jh} \begin{bmatrix} \int_0^1 e^{i\omega h(t-1)} t dt \\ \int_0^1 e^{i\omega h t} (1-t) dt \end{bmatrix}$$

where the basis functions are scaled to the master element  $\hat{\Omega} = [0, 1]$ . So,

$$\begin{aligned} \tau_h e_\omega &= \left( \hat{L}_h(\omega) \begin{bmatrix} 1 \\ 1 \end{bmatrix} - h \begin{bmatrix} \int_0^1 e^{i\omega h(t-1)} t dt \\ \int_0^1 e^{i\omega h t} (1-t) dt \end{bmatrix} \omega^2 \right) e^{i\omega jh} \\ &=: (\hat{L}_h(\omega) \hat{R}_h(\omega) - \hat{R}_h(\omega) \hat{L}(\omega)) e^{i\omega jh} \end{aligned} \tag{14}$$

where  $\hat{L}_h(\omega)$  is the Fourier transform of the block-Toeplitz matrix  $L_h$  for the point-wise stencil. The order of the truncation error is found by expansion of (14) for  $h \rightarrow 0$ . Since  $e_\omega = e^{i\omega x}$  is continuous, both for Baumann’s method ( $\sigma = 1, \mu = 0$ ), and for the symmetric DG-method without penalty ( $\sigma = -1, \mu = 0$ ) and with interior penalty ( $\sigma = -1, \mu = \nu/h$ ), the absolute value of the truncation error is

$$|\tau e_\omega| = \begin{bmatrix} \frac{1}{6} h^2 \omega^3 + O(h^3 \omega^4) \\ \frac{1}{6} h^2 \omega^3 + O(h^3 \omega^4) \end{bmatrix} \tag{15}$$

Table II. The expansion of (16) for  $h \rightarrow 0$ , i.e. the order of convergence of pointwise values at the nodal points.

IP, $\mu = 1/h$	IP, $\mu = \nu/h, \nu > 1$
$\begin{pmatrix} -\frac{1}{3} h\omega + O(h^2 \omega^2) \\ +\frac{1}{3} h\omega + O(h^2 \omega^2) \end{pmatrix}$	$\begin{pmatrix} -\frac{1}{12(\nu-1)} h^3 \omega^3 + O(h^4 \omega^4) \\ +\frac{1}{12(\nu-1)} h^3 \omega^3 + O(h^4 \omega^4) \end{pmatrix}$

However, from the previous section we know that only the IP DG-method is stable and definite, provided we choose  $\nu \geq 1$ . So, for that method we can derive the discrete convergence from

$$L_h^{-1} \tau_h e_\omega = \widehat{L}_h^{-1}(\omega) (\widehat{L}_h(\omega) \widehat{R}_h(\omega) - \widehat{R}_h(\omega) \widehat{L}(\omega)) e^{i\omega j h} \quad (16)$$

The results are summarized in Table II, distinguishing between penalty parameters  $\mu = 1/h$  and  $\mu = \nu/h$  with  $\nu > 1$ . We see that we lose two orders of accuracy if  $\mu = 1/h$ . The IP DG-method is more accurate for a larger constant  $\nu$ , but on the other hand, the method becomes less attractive due to the worse condition number of the discrete operator  $L_h$ .

#### 4. SMOOTHING ANALYSIS AND CONVERGENCE OF THE TWO-LEVEL ALGORITHM

In this section we consider three block-relaxation methods: Jacobi-, Gauss–Seidel-, and symmetric Gauss–Seidel block relaxations. If we want to apply these relaxations to the unstable operators (Baumann or symmetric DG with  $\mu = 0$ ) with *cell-wise blocks*, then we notice that (i) it is impossible to apply Jacobi relaxation because of the singular diagonal blocks, and (ii) that block GS does not converge because all eigenvalues of the iteration operator have absolute value equal to 1. *Point-wise* block relaxation can be used. However, as can be expected, spurious modes remain and no smoothing is achieved.

For the stabilized methods, with  $\mu \geq 1/h$ , all block relaxations are smoothers, but for  $\mu > 1/h$  point-wise block methods perform much better than the cell-wise block equivalents.

Because of this result, later in this section we drop the *cell-wise* relaxation and analyze two-level convergence for each of the three *point-wise* block relaxations. We determine the spectrum of the two-level iteration operator (for different values of  $\mu$ ) and compute for each of the relaxations the optimal damping parameter and the corresponding convergence rate.

Finally, in order to show that fast convergence is not only an asymptotic property after many iterations, but can be expected already in the first steps, we determine the spectral norms for the iteration operators at the end of Section 4.2.

##### 4.1. Smoothing analysis

Having shown in Reference [9] for piecewise cubics that the smoothing properties of the damped block-Jacobi (JOR) and the damped block-Gauss–Seidel (DGS) are better for point-wise ordering than for cell-wise ordering, we see the same for piecewise linear basis functions.

Table III. The relaxation methods.

$\alpha > 0$  is a damping parameter

	$B_h$	$M_h^{\text{REL}}$
JOR	$\alpha D^{-1}$	$D^{-1}((1 - \alpha)D - \alpha(L + U))$
DGS <sub>L</sub>	$\alpha(D + L)^{-1}$	$(D + L)^{-1}((1 - \alpha)(D + L) - \alpha U)$
DGS <sub>U</sub>	$\alpha(D + U)^{-1}$	$(D + U)^{-1}((1 - \alpha)(D + U) - \alpha L)$

Table IV. The stencils in the diagonal decomposition.

Cell-wise		Point-wise
$\frac{1}{h} \begin{bmatrix} -\frac{1}{2} & \frac{1-\sigma}{2} - h\mu \\ 0 & \frac{1}{2}\sigma \end{bmatrix}$	$L$	$\frac{1}{h} \begin{bmatrix} \frac{1}{2}\sigma & \frac{-1-\sigma}{2} \\ 0 & -\frac{1}{2} \end{bmatrix}$
$\frac{1}{h} \begin{bmatrix} \frac{1+\sigma}{2} + h\mu & \frac{-1-\sigma}{2} \\ \frac{-1-\sigma}{2} & \frac{1+\sigma}{2} + h\mu \end{bmatrix}$	$D$	$\frac{1}{h} \begin{bmatrix} \frac{1+\sigma}{2} + h\mu & \frac{1-\sigma}{2} - h\mu \\ \frac{1-\sigma}{2} - h\mu & \frac{1+\sigma}{2} + h\mu \end{bmatrix}$
$\frac{1}{h} \begin{bmatrix} \frac{1}{2}\sigma & 0 \\ \frac{1-\sigma}{2} - h\mu & -\frac{1}{2} \end{bmatrix}$	$U$	$\frac{1}{h} \begin{bmatrix} -\frac{1}{2} & 0 \\ \frac{-1-\sigma}{2} & \frac{1}{2}\sigma \end{bmatrix}$

In this section we analyze the different smoothers for the linear case, again distinguishing between the cell-wise (7) and point-wise (8) approach.

For the discrete system  $A_h x = b$  we consider the iterative process

$$x^{(i+1)} = x^{(i)} - B_h(A_h x^{(i)} - b) \tag{17}$$

with  $B_h$  an approximate inverse of  $A_h$ . Decomposing  $A_h$  as

$$A_h = L + D + U \tag{18}$$

into a strictly block-lower, a block-diagonal and a strictly block-upper matrix, the different relaxation methods are uniquely described either by  $B_h$  or by the amplification matrix  $M_h^{\text{REL}} = I_h - B_h A_h$ . These operators are shown in Table III. Because  $A_h$  is a block-Toeplitz operator, also the amplification matrix  $M_h$  is block Toeplitz. Notice, that the meaning of the block decomposition (18) is different for the stencils (7) and (8). The stencils corresponding to the decomposition (18) are given in Table IV. As we emphasized in Reference [9], the difference between cell-wise and point-wise decomposition is that the eigenvectors  $e_{h,\omega}(mh)\mathbf{v}$

of the cell-wise stencil correspond to two-valued grid functions associated with the cell interiors (in fact independently of the basis chosen), whereas for the point-wise stencil they correspond to the two-valued grid function with *the nodal points* between the cells. This makes the point-wise stencil better suited for a multi-grid algorithm. Using (9) we find the Fourier transform of the basic Toeplitz operators:  $\hat{L}(\omega) = Le^{-i\omega h}$ ,  $\hat{D}(\omega) = D$ ,  $\hat{U}(\omega) = Ue^{i\omega h}$ . This yields the Fourier transform for the amplification operators for JOR, DGS and SGS:

$$\widehat{M}_{\text{JOR}}^{\text{REL}} = \hat{D}^{-1}((1 - \alpha)\hat{D} - \alpha(\hat{L} + \hat{U})) \quad (19)$$

$$\widehat{M}_{\text{DGS}_L}^{\text{REL}} = (\hat{D} + \hat{L})^{-1}((1 - \alpha)(\hat{D} + \hat{L}) - \alpha\hat{U}) \quad (20)$$

$$\widehat{M}_{\text{DGS}_U}^{\text{REL}} = (\hat{D} + \hat{U})^{-1}((1 - \alpha)(\hat{D} + \hat{U}) - \alpha\hat{L}) \quad (21)$$

$$\widehat{M}_{\text{SGS}}^{\text{REL}} = \widehat{M}_{\text{DGS}_L}^{\text{REL}} \widehat{M}_{\text{DGS}_U}^{\text{REL}} \quad (22)$$

By (11) we find the eigenvalues of  $M_h^{\text{REL}}$  by computing the eigenvalues of  $\widehat{M}_h^{\text{REL}}(\omega)$  for  $\omega \in \mathbb{T}_h$ . The eigenvalues corresponding with the high frequencies ( $|\omega| > \pi/2h$ ), that determine the smoothing properties of the relaxation, are found as  $\widehat{M}_h^{\text{REL}}(\omega)$  for  $\omega \in \mathbb{T}_h \setminus \mathbb{T}_{2h}$ . The spectra for the three different smoothers, applied on the DG method of Baumann ( $\sigma = 1$ ,  $\mu = 0$ ), the symmetric DG-method ( $\sigma = -1$ ,  $\mu = 0$ ) and the IP-DG-method ( $\sigma = -1$ ,  $\mu = \nu/h$ ) are shown in the Figures 2–4, respectively.

The IP-DG-method is stable for penalty parameters  $\mu = \nu/h$ ,  $\nu \geq 1$ , which is reflected in the fact that the only undamped mode is the constant (eigen)function.

In Figures 2–4 we see that the Baumann and the symmetric DG method (both with  $\mu = 0$ ) show their instability by not damping the highest frequencies  $|\omega| \approx \pi/h$ . The high frequencies appear to be handled similarly as the low frequencies. We see that the IP-DG methods allow smoothing by the various relaxation methods, and that (the case  $\mu = 1/h$  excluded) the point-wise relaxations are better than the cell-wise relaxations (high frequencies are better damped).

In Table V we summarize the damping of the high frequencies and we show the corresponding optimal damping factors,  $\alpha$ , and smoothing factors for the damped relaxation methods in point-wise setting. We conclude that the pointwise block-relaxation methods are excellent smoothers. This brings us to focus more on their behavior in a multigrid algorithm in the next section.

#### 4.2. The two-level analysis (TLA)

Now we study the two-level operator for the IP-DG-method with three choices of  $\mu$ , viz.  $\mu = 1/h$ ,  $2/h$  and  $5/h$ , and we will compute optimal damping parameters for the smoothers JOR, DGS and SGS in combination with the coarse-grid correction (CGC) for the different choices of the parameter  $\mu$ . The amplification operator of the two-level algorithm for the error is given by

$$\begin{aligned} M_h^{\text{TLA}} &= (M_h^{\text{REL}})^{\nu_2} M_h^{\text{CGC}} (M_h^{\text{REL}})^{\nu_1} \\ &= (M_h^{\text{REL}})^{\nu_2} (I - P_{hH} L_H^{-1} \tilde{R}_{Hh} L_h) (M_h^{\text{REL}})^{\nu_1} \end{aligned}$$

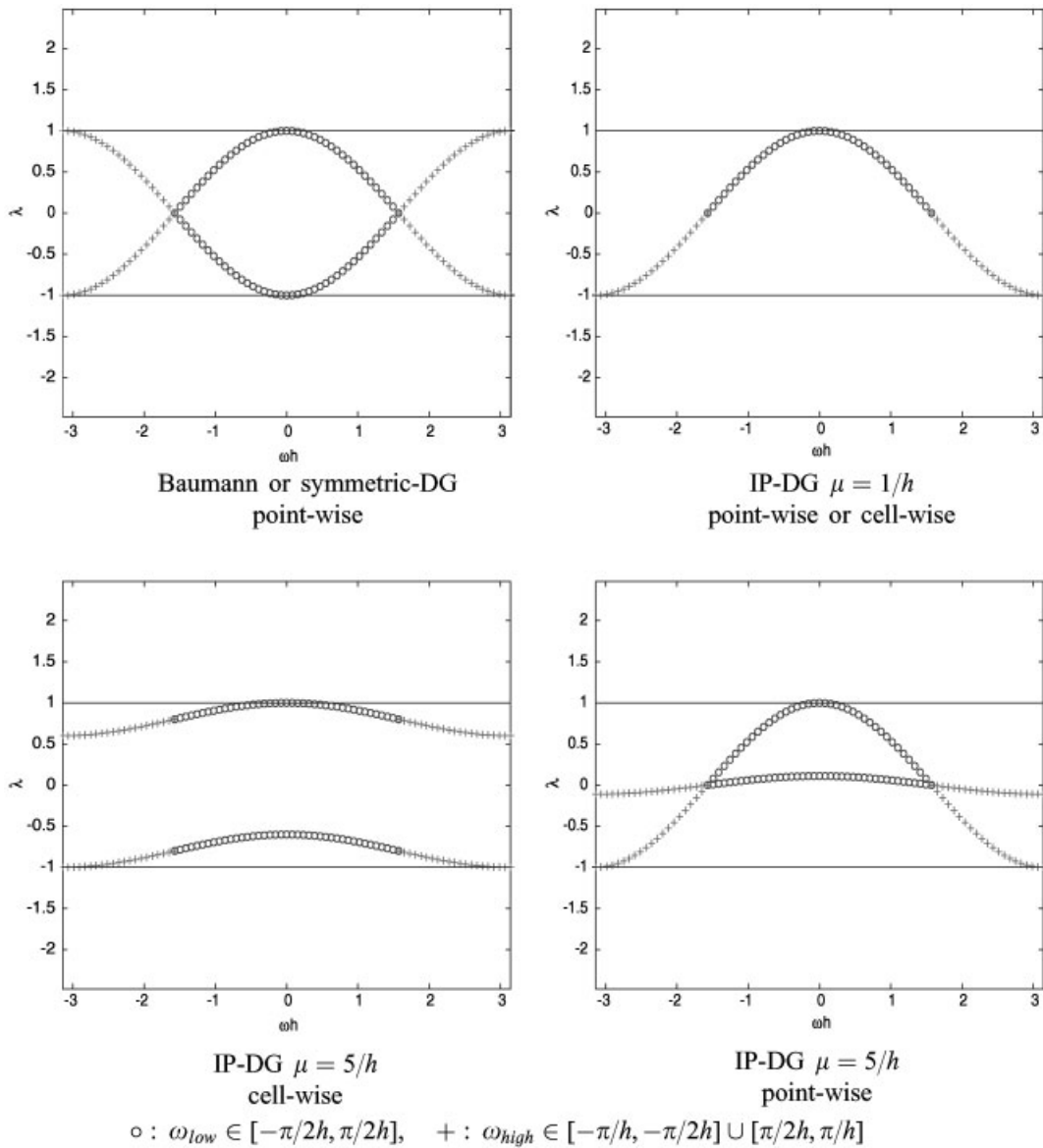


Figure 2. Eigenvalue spectra of  $\widehat{M}_{JOR}^{REL}(\omega)$ .

where  $v_1$  and  $v_2$  are the number of pre- (post-) relaxation sweeps, respectively.  $M_h^{CGC}$  is the amplification operator of the CGC. The amplification operator for the residue is

$$\begin{aligned} \bar{M}_h^{TLA} &= (\bar{M}_h^{REL})^{v_2} \bar{M}_h^{CGC} (\bar{M}_h^{REL})^{v_1} \\ &= (L_h M_h^{REL} L_h^{-1})^{v_2} L_h M_h^{CGC} L_h^{-1} (L_h M_h^{REL} L_h^{-1})^{v_1} \end{aligned}$$

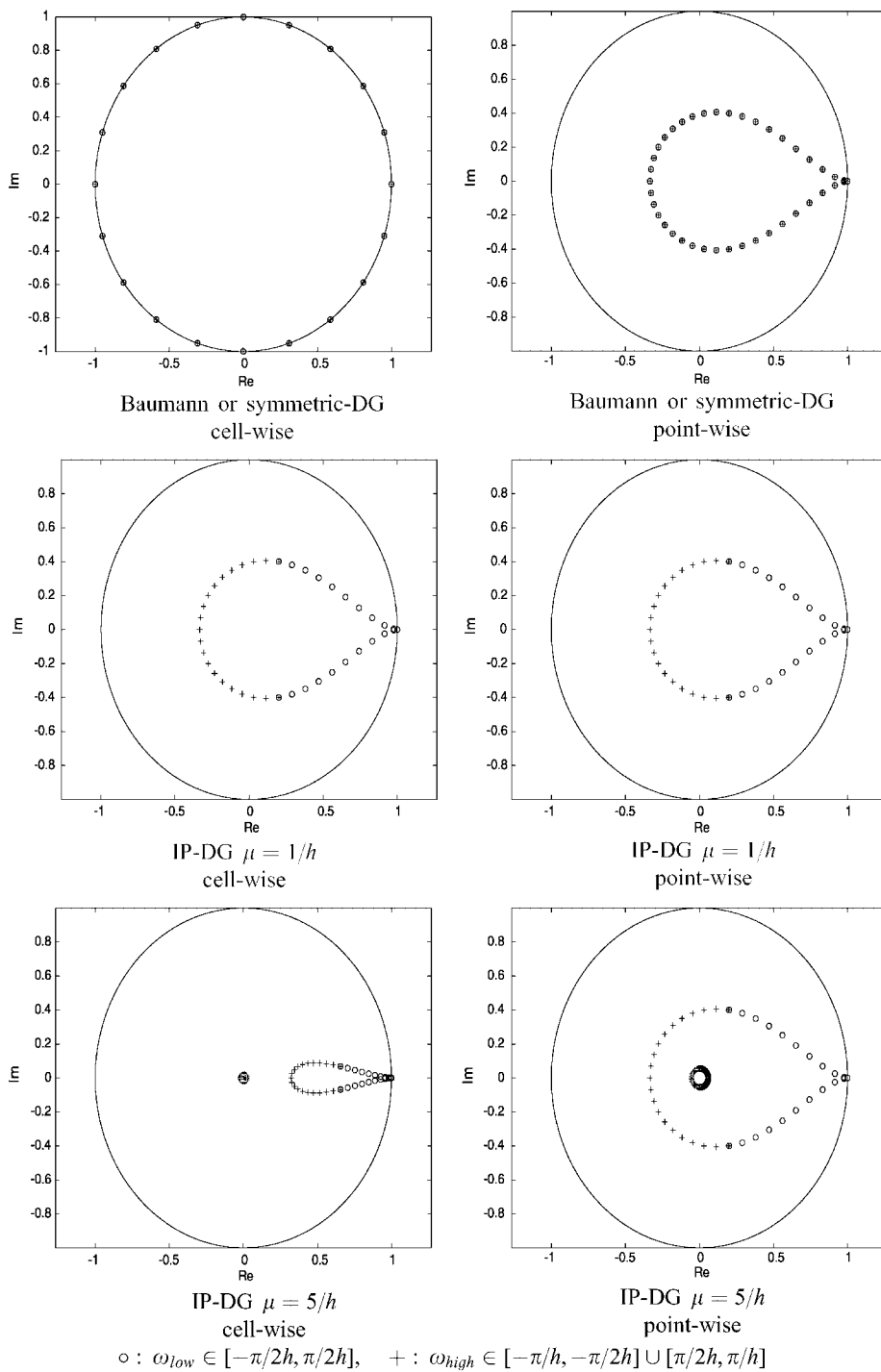


Figure 3. Eigenvalue spectra of  $\widehat{M}_{DGS}^{REL}(\omega)$ , without damping ( $\alpha=1$ ) relative to unit circle.

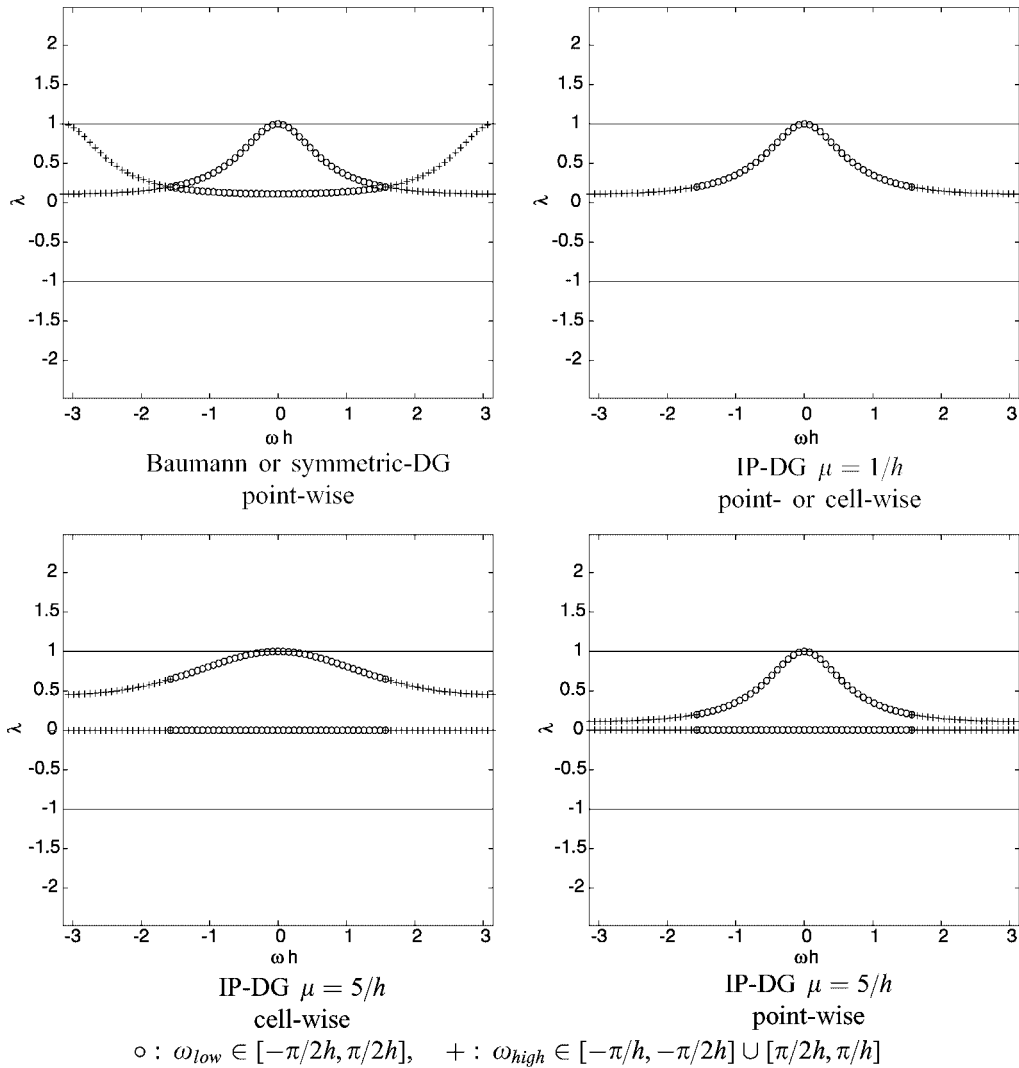


Figure 4. Eigenvalue spectra of  $M_{SGS}^{REL}(\omega)$ .

It follows from Reference [9] that the Fourier transform of the CGC  $M_h^{CGC}$  is

$$\begin{aligned}
 \widehat{M}_h^{CGC}(\omega) &= (\widehat{I}_h - \widehat{P}_{hH} \widehat{L}_H^{-1} \widehat{R}_{Hh} \widehat{L}_h)(\omega) = \begin{pmatrix} 1 & 0 \\ 0 & 1 \end{pmatrix} \\
 &\quad - \begin{pmatrix} \widehat{P}_h(\omega) \\ \widehat{P}_h(\omega + \pi/h) \end{pmatrix} (\widehat{L}_H(\omega))^{-1} (\widehat{R}_h(\omega) \quad \widehat{R}_h(\omega + \pi/h)) \begin{pmatrix} \widehat{L}_h(\omega) & 0 \\ 0 & \widehat{L}_h(\omega + \pi/h) \end{pmatrix}
 \end{aligned}$$

Table V. Smoothing factors ( $\text{sf} = \max_{\pi/2h \leq |\omega| \leq \pi/h} |\lambda(\omega)|$ ) for the undamped (top) and the damped (bottom) relaxation methods. The damped relaxations are shown only for their point-wise ordered versions, and the damping factor ( $\alpha$ ) is shown.

$\max_{\omega}  \lambda(\omega) $	JOR		DGS		SDGS	
	Cell	Point	Cell	Point	Cell	Point
$\pi/2h \leq  \omega  \leq \pi/h$						
Baumann	—	1.0	1.0	1.0	1.0	1.0
Symmetric DG	—	1.0	1.0	1.0	1.0	1.0
IP $\mu = 1/h$	1.0	1.0	0.447	0.447	0.200	0.200
IP $\mu = 5/h$	1.0	1.0	0.659	0.447	0.647	0.200
IP point-wise	$\alpha$	sf	$\alpha$	sf	$\alpha$	sf
$\mu = 2/h$	0.667	0.333	1.0	0.447	1.0	0.200
$\mu = 5/h$	0.667	0.333	1.0	0.447	1.0	0.200

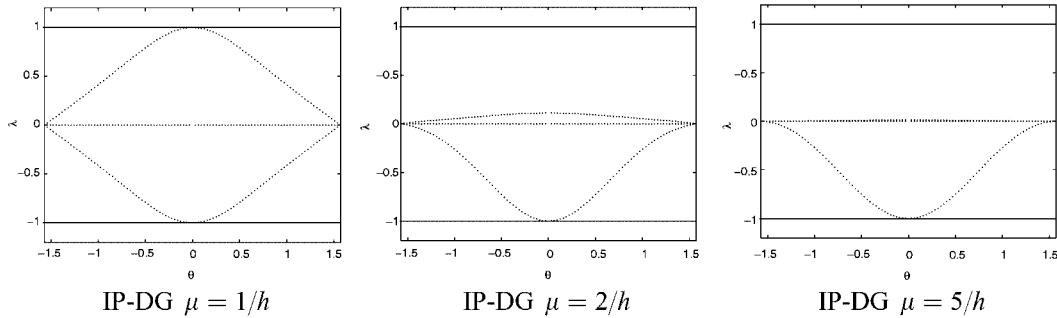


Figure 5. Eigenvalue spectra of  $\text{FT}(M_h^{\text{CGC}} M_{\text{JOR}}^{\text{REL}})(\omega) = \text{FT}(\tilde{M}_h^{\text{CGC}} \tilde{M}_{\text{JOR}}^{\text{REL}})(\omega)$ , without damping ( $\alpha = 1$ ).

For our piecewise linear basis  $\phi_{i,e}$ , the interpolation  $P_{hH} : S_H \rightarrow S_h$  so that  $(P_{hH} u_H)(x) = u_H(x)$  for all  $x \in \mathbb{R} \setminus \mathbb{Z}_h$ , is given by the stencil (for pointwise ordering):

$$P_{hH} \cong \left[ \begin{array}{c|cc|cc} 0 & \frac{1}{2} & 1 & 0 & \frac{1}{2} & 0 \\ \hline 0 & \frac{1}{2} & 0 & 1 & \frac{1}{2} & 0 \end{array} \right]$$

Because the DG discretization is of Galerkin type with equal test and trial space, the restriction of the residue,  $\tilde{R}_{Hh}$ , is the adjoint of the prolongation,  $\tilde{R}_{Hh} = (P_{hH})^T$ . For the different penalty parameters  $\mu$  and different smoothers JOR, DGS and SGS, the eigenvalue spectra of the two-level operator for the IP-DG-method are computed from (11) and shown in Figures 5–7.

We see that none of the methods converge for  $\mu = 1/h$ . However, for  $\mu = 2/h$  or  $5/h$  all pointwise relaxations are excellent smoothers and we see fast convergence for the two-level algorithm.

Having found the spectra and having computed the largest and smallest real eigenvalue  $\lambda_{\min}$  and  $\lambda_{\max}$  we can determine the optimal damping parameter and the corresponding convergence rate for the damped relaxation method. The parameter, minimizing the spectral radius

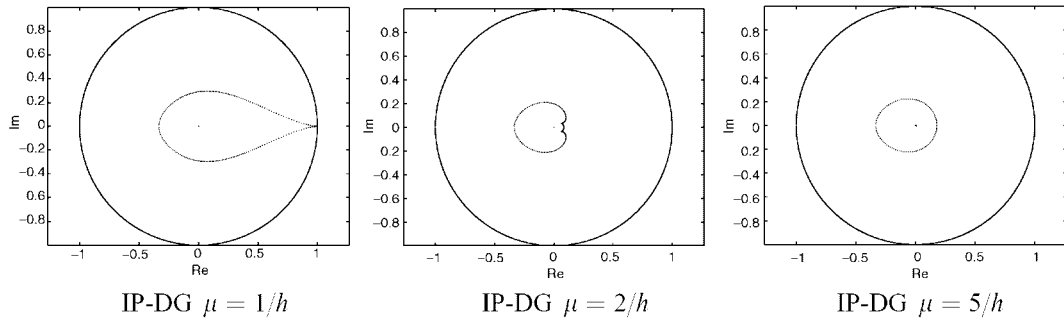


Figure 6. Eigenvalue spectra of  $FT(M_h^{CGC} M_{DGS}^{REL})(\omega) = FT(\tilde{M}_h^{CGC} \tilde{M}_{DGS}^{REL})(\omega)$ , without damping ( $\alpha = 1$ ).

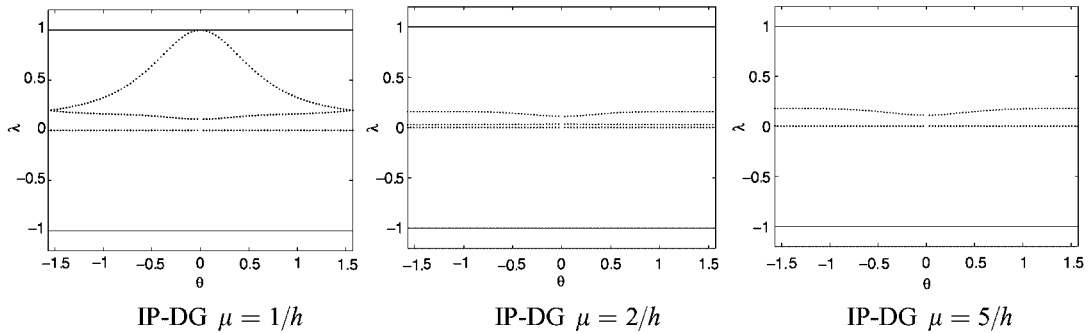


Figure 7. Eigenvalue spectra of two-level iteration with symmetric block-GS relaxation:

$$FT(M_{DGS_U}^{REL} M_h^{CGC} M_{DGS_L}^{REL})(\omega) = FT(\tilde{M}_{DGS_U}^{REL} \tilde{M}_h^{CGC} \tilde{M}_{DGS_L}^{REL})(\omega), \text{ without damping } (\alpha = 1).$$

Table VI. Damping parameters for the two-level operators  $\rho(M_h^{CGC} M_h^{REL}) = \rho(\tilde{M}_h^{REL} \tilde{M}_h^{CGC})$ .

$\alpha_{opt}$	IP-DG $\mu = 2/h$	IP-DG $\mu = 5/h$
$M_h^{CGC} M_{J\ddot{O}R}^{REL}$	0.692	0.669
$M_h^{CGC} M_{DGS}^{REL}$	0.897	0.928

$\rho(M_h^{CGC} M_h^{REL})$  is given by

$$\alpha_{opt} = \frac{2}{2 - (\lambda_{min} + \lambda_{max})}$$

Seeing that the case  $\nu = 1$  will not show  $h$ -independent convergence, we show in the Tables VI and VII the damping parameters and the convergence rates for the cases  $\nu = 2$  and 5.

In order not only to know the asymptotic convergence rate but also the guaranteed converge behavior after one or two iteration sweeps, we also compute the spectral norms  $\|M_h^{TLA}\|$ ,  $\|\tilde{M}_h^{TLA}\|$ ,  $\|(\tilde{M}_h^{TLA})^2\|$ . The results are shown in Tables VIII–X. We see that the two-level

Table VII. Spectral radii  $\rho(M_h^{\text{CGC}}M_h^{\text{REL}}) = \rho(\bar{M}_h^{\text{REL}}\bar{M}_h^{\text{CGC}})$  for damping parameters in Table VI.

$\rho(M_h^{\text{CGC}}M_h^{\text{REL}})$	IP-DG $\mu = 2/h$	IP-DG $\mu = 5/h$
$M_h^{\text{CGC}}M_{\text{JOR}}^{\text{REL}}$	0.385	0.339
$M_h^{\text{CGC}}M_{\text{DGS}}^{\text{REL}}$	0.217	0.238
$M_{\text{DGS}_U}^{\text{REL}}M_h^{\text{CGC}}M_{\text{DGS}_L}^{\text{REL}}$	0.156	0.180

Table VIII. The spectral norm ( $\sigma_{\max}$ ) after one iteration for the error with optimal damping.

	$M_h^{\text{CGC}}M_{\text{JOR}}^{\text{REL}}$	$M_h^{\text{CGC}}M_{\text{DGS}}^{\text{REL}}$	$M_{\text{DGS}_U}^{\text{REL}}M_h^{\text{CGC}}M_{\text{DGS}_L}^{\text{REL}}$
IP-DG ( $\mu = 2/h$ )	0.543	0.392	0.207
IP-DG ( $\mu = 5/h$ )	0.478	0.417	0.250

Table IX. The spectral norm ( $\sigma_{\max}$ ) after one iteration for the residue with optimal damping.

	$\bar{M}_h^{\text{CGC}}\bar{M}_{\text{JOR}}^{\text{REL}}$	$\bar{M}_h^{\text{CGC}}\bar{M}_{\text{DGS}}^{\text{REL}}$	$\bar{M}_{\text{DGS}_U}^{\text{REL}}\bar{M}_h^{\text{CGC}}\bar{M}_{\text{DGS}_L}^{\text{REL}}$
IP-DG ( $\mu = 2/h$ )	1.071	1.019	0.340
IP-DG ( $\mu = 5/h$ )	1.056	1.028	0.343

Table X. The spectral norm ( $\sigma_{\max}$ ) after two iterations for the residue with optimal damping.

	$\bar{M}_h^{\text{CGC}}\bar{M}_{\text{JOR}}^{\text{REL}}$	$\bar{M}_h^{\text{CGC}}\bar{M}_{\text{DGS}}^{\text{REL}}$	$\bar{M}_{\text{DGS}_U}^{\text{REL}}\bar{M}_h^{\text{CGC}}\bar{M}_{\text{DGS}_L}^{\text{REL}}$
IP-DG ( $\mu = 2/h$ )	0.411	0.200	0.030
IP-DG ( $\mu = 5/h$ )	0.357	0.244	0.035

algorithm (and hence the multi-level algorithm) converges with a rate of about 0.2–0.4 per iteration step and that reduction of the error and the residual is guaranteed, starting from the second iteration step.

## 5. NUMERICAL RESULTS

In this section we check by numerical experiments the spectral radii of the two-level operators with damped Jacobi-,  $M_h^{\text{CGC}}M_{\text{JOR}}^{\text{REL}}$ , Gauss–Seidel-,  $M_h^{\text{CGC}}M_{\text{DGS}}^{\text{REL}}$ , and symmetric Gauss–Seidel relaxation,  $M_{\text{DGS}_U}^{\text{REL}}M_h^{\text{CGC}}M_{\text{DGS}_L}^{\text{REL}}$ , for the IP-DG method with the penalty parameters  $\mu = 2/h$  and  $5/h$ . For that purpose we consider an inhomogeneous Poisson equation

$$-u_{xx} = \frac{e^{x/\varepsilon}}{\varepsilon^2(\varepsilon^{1/\varepsilon} - 1)} \quad \text{with } u(0) = 0, \quad u(1) = 0, \quad \varepsilon = 1/64$$

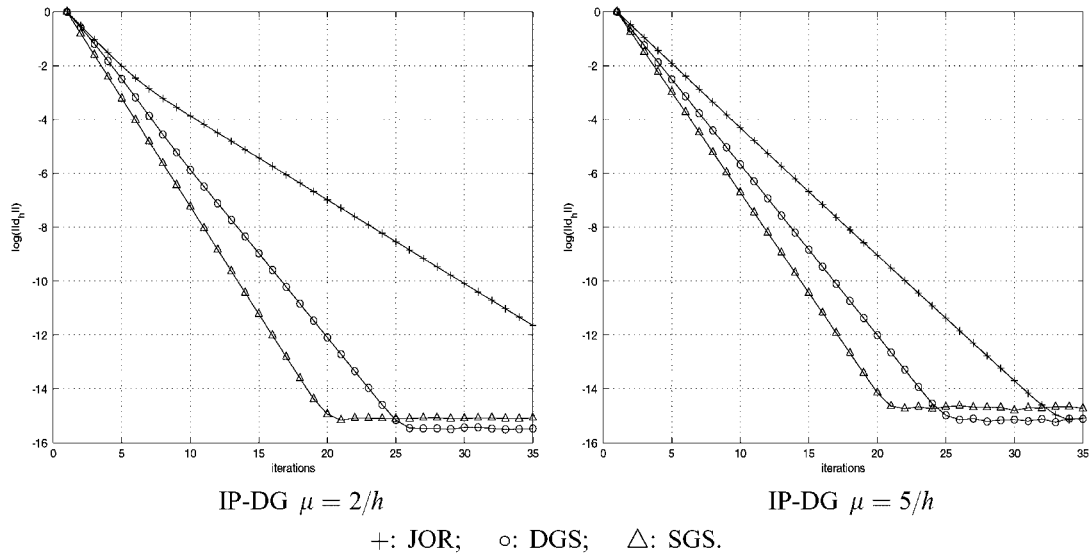


Figure 8.  $\log(\|d_h\|_2)$  as function of iterations for the two-level iteration operator on the error.

which has a sharp boundary layer-type solution. For the discrete system we use the linear basis polynomials and we set the meshwidth to  $h=2^{-6}$ . Our initial approximation is the grid-function  $u_h^0 = u_{h,\text{PRE}}^0 = \sin(1/2\pi j)$ . We apply a pre-relaxation sweep

$$u_{h,\text{PRE}}^{i+1} = u_{h,\text{PRE}}^i + B_h(f_h - L_h u_{h,\text{PRE}}^i)$$

with  $B_h$  the approximate inverse of  $L_h$  as given in Table III, and the coarse-grid correction

$$u_{h,\text{POST}}^0 = u_{h,\text{PRE}}^{v_1} + P_{hH} L_H^{-1} \bar{R}_{Hh}(f_h - L_h u_{h,\text{PRE}}^{v_1})$$

In case of symmetric damped Gauss–Seidel we apply an additional post relaxation sweep

$$u_{h,\text{POST}}^{i+1} = u_{h,\text{POST}}^i + B_h^T(f_h - L_h u_{h,\text{POST}}^i)$$

To be consistent with the Fourier analysis we measure the residue in the 2-norm

$$\|d_h\|_2 = \|f_h - L_h u_h\|_2 = \left( \sum_{e=1}^{64} \sum_{j=1}^2 d_{h,e,j}^2 \right)^{1/2}$$

The convergence of the residue is shown in Figure 8. The convergence factors as observed, are given in Table XI.

Both for  $\mu=2/h$  and  $5/h$  we see convergence, starting from the first iteration sweep. Furthermore, for the IP-DG method with  $\mu=5/h$  the observed convergence factors correspond very well to the spectral radii shown in Table VII. Only for the IP-DG method with  $\mu=2/h$  the spectral radii of the Fourier analysis seem too optimistic compared with the convergence factors in Table XI. This is clearly caused by a boundary effect (as can be seen if we study the slowest converging component, which is exponentially growing towards the boundary).

Table XI. Numerically obtained convergence factors corresponding with  $\rho(M_h^{\text{CGC}} M_h^{\text{REL}}) = \rho(\tilde{M}_h^{\text{REL}} \tilde{M}_h^{\text{CGC}})$  for damping parameters as in Table VI.

$\rho(M_h^{\text{CGC}} M_h^{\text{REL}})$	IP-DG $\mu = 2/h$	IP-DG $\mu = 5/h$
$M_h^{\text{CGC}} M_{\text{JOR}}^{\text{REL}}$	0.48	0.34
$M_h^{\text{CGC}} M_{\text{DGS}}^{\text{REL}}$	0.24	0.23
$M_{\text{DGS}_U}^{\text{REL}} M_h^{\text{CGC}} M_{\text{DGS}_L}^{\text{REL}}$	0.17	0.18

This is related to the fact that, as  $\mu$  approaches  $1/h$ , the two-level algorithm becomes singular. This singularity effect disappears for larger values of  $\nu = h\mu$ .

## 6. CONCLUSION

In an earlier paper we have shown that multigrid iteration can be quite efficient for the solution of elliptic equations that are discretized by higher-order discontinuous Galerkin discretization, provided that a block (Jacobi or Gauss–Seidel) relaxation is used, based on a point-wise (instead of a cell-wise) ordering.

In this paper we have studied the solution of the discrete equations for the discontinuous Galerkin method with piecewise linear test- and trial functions. It is well known [10, 11] that in this case the DG method requires an interior penalty (IP) parameter  $\mu > 1$  in order to guarantee that the discrete equations are stable.

We show that in this case, again, a multigrid method can be used to solve the corresponding discrete equations if block relaxation is used, based on the pointwise ordering. If a suitable IP parameter  $\mu > 1$  is chosen, the block Jacobi or (symmetric) block Gauss–Seidel relaxation have a good smoothing property.

Using Fourier analysis, in this paper, for feasible  $\mu$ -values, we compute optimal damping parameters for the relaxation methods and the corresponding two-level convergence rates. In view of the hierarchical structure of the DG multigrid-algorithm proposed in Reference [9], the present results can also be used to justify the use of a low-order discretization in the hierarchical scale of methods, if needed.

## REFERENCES

1. Cockburn B. *Discontinuous Galerkin Methods for Convection Dominated Problems*, 1999. Lecture Notes, available at <http://www.math.umn.edu/~cockburn/LectureNotes.html>.
2. Cockburn B, Shu CW. The local finite element method for convection-diffusion systems. *SIAM Journal on Numerical Analysis* 1998; **35**:2440–2463.
3. Houston P, Schwab C, Süli E. Discontinuous *hp*-finite element methods for advection-diffusion problems. *Technical Report No. 2000-07*, ETHZ, Zürich, Switzerland, 2000.
4. Arnold DN, Brezzi F, Cockburn B, Marini D. Unified analysis of discontinuous Galerkin methods for elliptic problems. *SIAM Journal on Numerical Analysis* 2002; **39**:1749–1779.
5. Oden JT, Babuška I, Baumann CE. A discontinuous *hp* finite element method for diffusion problems. *Journal of Computational Physics* 1998; **146**:491–519.
6. Baumann CE, Oden JT. *An hp-adaptive Discontinuous Finite Element Method for Computational Fluid Dynamics*. The University of Texas: Austin, 1997.

7. Süli E, Houston P, Schwab C. *hp*-finite element methods for hyperbolic problems. In *Highlights of the MAFFELAP X Conference*, Whiteman J (ed.). Uxbridge, 1999. World Scientific Publishers: Singapore, 1999.
8. Süli E, Schwab C, Houston P. *hp*-DGFEM for partial differential equations with nonnegative characteristic form. In *Proceedings of the International Symposium on Discontinuous Galerkin Methods*, Cockburn B, Karniadakis GE, Shu CW (eds). Newport, RI, Lecture Notes in Computational Science and Engineering, vol. 11, 2000; 221–230.
9. Hemker PW, Hoffmann W, van Raalte MH. Two-level Fourier analysis of a multigrid approach for discontinuous Galerkin discretisation. *Technical Report MAS-R0206*, CWI, Amsterdam, April 2002. to appear in *SIAM Journal on Scientific Computing*.
10. Arnold DN. An interior penalty finite element method with discontinuous elements. *SIAM Journal on Numerical Analysis* 1982; **19**:742.
11. Rivière B, Wheeler MF, Girault V. Improved energy estimates for interior penalty, constrained and discontinuous Galerkin methods for elliptic problems. Part I. *Computational Geosciences* 1999; **3**:337–360.
12. Wheeler MF. An elliptic collocation-finite element method with interior penalties. *SIAM Journal on Numerical Analysis* 1978; **15**:152.